Orientation-Compensative Signal Registration for Owner Authentication Using an Accelerometer

Trung Thanh NGO[†a], **Yasushi MAKIHARA**[†], *Nonmembers*, **Hajime NAGAHARA**[††], **Yasuhiro MUKAIGAWA**[†], *and* **Yasushi YAGI**[†], *Members*

SUMMARY   Gait-based owner authentication using accelerometers has recently been extensively studied owing to the development of wearable electronic devices. An actual gait signal is always subject to change due to many factors including variation of sensor attachment. In this research, we tackle to the practical sensor-orientation inconsistency, for which signal sequences are captured at different sensor orientations. We present an iterative signal matching algorithm based on phase-registration technique to simultaneously estimate relative sensor-orientation and register the 3D acceleration signals. The iterative framework is initialized by using 1D orientation-invariant resultant signals which are computed from 3D signals. As a result, the matching algorithm is robust to any initial sensor-orientation. This matching algorithm is used to match a probe and a gallery signals in the proposed owner authentication method. Experiments using actual gait signals under various conditions such as different days, sensors, weights being carried, and sensor orientations show that our authentication method achieves positive results.

key words: *biometric authentication, dynamic programming, gait, accelerometer, sensor-orientation inconsistency*

1. Introduction

Wearable and portable electronic devices are increasingly becoming useful to human life. They have rapidly become more and more sophisticated to interact with their owners and understand their needs, intentions or actions [1]–[3], and health conditions [4]–[6]. Accelerometers are increasingly being embedded in devices such as smartphones, tablets, and smartwatches, and owner assistance from smartphones has recently become an active research topic [7]–[12].

A useful source of information for assisting an owner is his/her gait (walking) signal, because the human gait conveys a variety of information such as personality [13], gender [14], physical or clinical condition [15], [16], and mood [17], and can easily be captured by accelerometers. In particular, personality in gait signal plays quite an important role when recognizing the person carrying the device.

There are many existing methods for recognizing a person carrying a sensor based on the gait signals of an inertial sensor, such as identification [7], [18]–[20] or authentication [21]–[26], which showed a promising application of inertial sensors for biometric recognition. Because the human

gait is a periodic motion, there are several approaches for gait-based owner recognition: gait model-based, frequency analysis-based, and period detection-based approaches. In the model-based methods [27], [28], gait signal is modeled by using a finite state machine then some characteristics such as the gait period symmetry and homogeneity are extracted as gait pattern. In the frequency analysis-based methods, a histogram of signal intensity [7], [29] or a vector of coefficients of Fourier, wavelet transform [19], [30] are used as a gait pattern. In the period detection-based methods [18]–[26], [31], [32], a gait period (two consecutive steps) is first detected, and the signal segment of the gait period is used as a gait pattern.

The most challenging problem of inertial sensor-based gait recognition methods is temporal distortion of signal. The problem is because human gait signals always vary owing to many natural covariates such as mood, physical condition, walking speed, ground condition, weight being carried, shoes, and so on. To solve this problem, some existing period detection-based methods [21], [24], [26] apply dynamic time warping (DTW) for signal matching to overcome the temporal distortion. Particularly, there exists a period detection-based method [21] that can overcome the distortion not only in signal matching but also in gait period detection. This method modifies the Self DTW [33] to accurately detect a period and remove the temporal distortion in constructing a gallery without any heuristic information, and thus achieved the best performance in large-scale evaluation in [34]. In contrast, the gait model-based and frequency analysis-based approaches do not work well against such distortion. The reason is that the gait model-based methods require an expert knowledge about the human gait to train the finite state machine, and hence they may fail when the input data is considerably deviated from the expert knowledge due to the variation. Meanwhile, since the frequency analysis-based methods require properly long and stable signal sequence to compute frequency coefficients or gait statistical characteristics, they may not work well with signals containing the temporal distortion induced by the covariates [19], [21], [25].

However, regardless of the approaches, sensor-orientation inconsistency poses a serious problem for matching between a probe and gallery signals. In detail, the sensor-orientation variation of sensor attachment does not actually make any temporal distortion but rotates the signals so that they cannot be matched properly. A solution to avoid

this problem is to fix the sensor on the owner's body as most existing methods [7], [18]–[29], [31], [32] do. However, it is undesirable and unnatural in real applications (e.g. it is inconvenient to have to place a smart phone in our pocket with exactly the same orientation from day to day). Moreover, even if the sensor is fixed on our body trunk, it is also difficult to permanently keep the same body's tilt. Therefore, it is essential to cope with sensor-orientation inconsistency problem for wearable sensor-based owner authentication.

In the frequency analysis-based methods, there exist solutions [29], [30] for the sensor-orientation inconsistency problem. Gafurov et al. [29] uses a histogram of signal magnitude as a gait pattern. A signal magnitude is a norm of a 3D acceleration signal, which is found invariant to sensor-orientation and called sensor orientation-invariant 1D resultant signal. Therefore, this method can solve the sensor-orientation inconsistency problem. However, a significant amount of information is lost in the temporal domain, which reduces the recognition performance. In [30], a 3D signal sequence is transformed into frequency space, and an autocorrelation matrix of the frequency matrix is computed. This autocorrelation matrix is invariant to initial sensor-orientation. Then, a gait pattern extracted from this matrix is also invariant to sensor-orientation. However, compared with the original signal, this autocorrelation matrix has a much larger number of dimensions. Which means a large amount of data from this matrix is redundant. Consequently, a supervised machine learning method is also used to select only some good features from this matrix, the quality of selected features depends on the quality of the training dataset. As a result, some information is lost in the frequency domain, which reduces the recognition performance similar to the above histogram-based method [29]. In addition, since these methods are frequency analysis-based methods, they also face the robustness problem of the temporal distortion as stated above.

In this paper, we tackle to the sensor-orientation inconsistency problem for period detection-based approach. We propose an iterative matching algorithm to simultaneously estimate signal correspondence and relative sensor-rotation between gallery and probe signals. While an initial signal correspondence is given by using a sensor-orientation-invariant 1D resultant signal, the proposed method uses full three dimensions of signals for matching without any information loss, unlike the existing orientation-invariant methods [29], [30]. For period detection, we apply the above mentioned period detection-based method [21] since it has a good performance [34] and can work with any initial sensor-orientation.

2. Preliminaries

2.1 Assumptions

In our research, the user who is carrying the sensor is assumed to walk at his/her normal speed on a flat ground. The gait signal is captured by a triaxial accelerometer attached to the same location on the subjects' body, either on the back, waist, or leg. For example, the sensor can be placed in a belt bag, backpack, or trouser pocket.

In an enrollment session, the sensor is assumed to be fixed on the body-part (e.g. on the back, waist, or leg) at an arbitrary initial sensor-orientation and then gallery gait patterns of one gait period are constructed for each user based on the method [21].

In an authentication session, we also assume that the sensor is relatively fixed on the body-part but only for a short term (e.g., one second) and its initial sensor-orientation may differ from that of the enrollment session. Thus, the sensor may be relatively fixed on the subject's body at different initial sensor-orientations among these short terms within the same authentication session (e.g., picking up a smartphone from a pocket and putting it into the pocket again or gradual change of the smartphone's orientation in the pocket).

In this paper, a fixation of the sensor means it is firmly attached on the body-part. The initial sensor-orientation is the orientation of the sensor coordinate system at an initial pose of the body (e.g. T-pose of the body) in a world coordinate system.

2.2 Problem Settings

In a fixed world coordinate system, the i-th sample of 3D acceleration of a subject's gait is described as vector $\boldsymbol{a}_i = \left(a_{x,i}, a_{y,i}, a_{z,i}\right)^T$. If an accelerometer is attached to the body of the subject, and the initial sensor-orientation of the sensor coordinate system is described by a rotation matrix $\boldsymbol{R}'$ as shown in Fig. 1, the sensor observes a different measurement $\boldsymbol{a}'_i = \left(a'_{x,i}, a'_{y,i}, a'_{z,i}\right)^T$ such that

$$\boldsymbol{a}'_i = \boldsymbol{R}'\boldsymbol{a}_i. \tag{1}$$

In the same way, rotation of a signal sequence $A = \{\boldsymbol{a}_i\}$ ($i = 0, \ldots, N - 1$) by a rotation matrix $\boldsymbol{R}'$ results in another signal sequence $A' = \{\boldsymbol{a}'_i\}$ ($i = 0, \ldots, N - 1$), where N is the number of samples in the sequence. This transform is defined as:
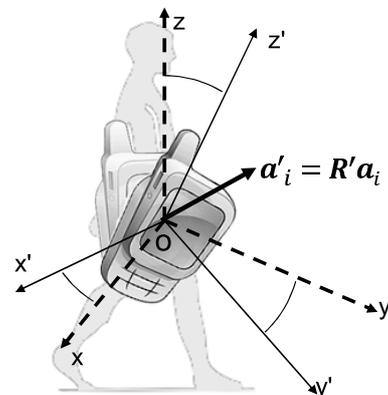

Fig. 1 Initial sensor-orientation inconsistency problem. The same human motion may be observed and captured with different signals due to different initial sensor-orientations.

$$\boldsymbol{R}' \odot \boldsymbol{A} := \{\boldsymbol{R}'\boldsymbol{a}_i\} = \boldsymbol{A}', \tag{2}$$

where $\odot$ is a rotation operator that is applied to a signal sequence.

Obviously, if we have another accelerometer, the initial sensor-orientation of which is described by a rotation matrix $\boldsymbol{R}''$, the measurement $\boldsymbol{a}_i'' = \left(a_{x,i}'', a_{y,i}'', a_{z,i}''\right)^T = \boldsymbol{R}''\boldsymbol{a}_i$ may differ from $\boldsymbol{a}_i'$, even though these accelerometers observe the same motion. Thus, in the recognition problem, we cannot directly compare signals captured with different sensor orientations.

Next, we consider matching a 3D gallery signal sequence $\boldsymbol{G} = \{\boldsymbol{g}_i\}$ ($\boldsymbol{g}_i \in \mathbb{R}^3; i = 0,\ldots,N_G - 1$) and a 3D probe signal sequence $\boldsymbol{P} = \{\boldsymbol{p}_j\}$ ($\boldsymbol{p}_j \in \mathbb{R}^3; j = 0,\ldots,N_P-1$). On the one hand, because the gallery and the probe signal sequences are captured with different initial sensor-orientations in general (e.g., represented by rotation matrices $\boldsymbol{R}_G$ and $\boldsymbol{R}_P$ for the gallery and the probe, respectively), such a relative sensor-orientation difference needs to be compensated before matching (e.g., preparing a orientation-compensated probe signal sequence $\boldsymbol{P}' = \boldsymbol{R}\boldsymbol{P}$, where $\boldsymbol{R} = (\boldsymbol{R}_G)(\boldsymbol{R}_P)^{-1}$, so as to match the initial sensor-orientation of the gallery signal sequence). On the other hand, the gallery and probe signal sequences are captured with different start phases (gait stances) and hence an appropriate signal correspondence $\boldsymbol{C} = \{(i_k, j_k)\}$ ($k = 0,\ldots,N_K - 1$) $= \{\boldsymbol{c}_k\}$ ($k = 0,\ldots,N_K - 1$) between the probe and gallery signal sequences needs to be acquired so as to synchronize the phases between them before matching, where $\boldsymbol{c}_k = (i_k, j_k)$ is a correspondence pair, the i_k-th sample of $\boldsymbol{G}$ corresponds to j_k-th sample of $\boldsymbol{P}$, and N_K is the number of correspondence pairs. Consequently, the problem is stated as simultaneous estimation of the relative rotation matrix $\boldsymbol{R}$ and the signal correspondence $\boldsymbol{C}$ for correct matching, given a pair of the gallery signal sequence $\boldsymbol{G}$ and probe signal sequence $\boldsymbol{P}$.

Generally, it is difficult to acquire the signal correspondence $\boldsymbol{C}$ directly without orientation-compensation, while it is also difficult to estimate the rotation matrix $\boldsymbol{R}$ without signal correspondence.

In other words, *if the relative rotation matrix $\boldsymbol{R}$ is known*, the probe signal sequence can be orientation-compensated as $\boldsymbol{P}' = \boldsymbol{R} \odot \boldsymbol{P}$, and dynamic programming techniques can then be applied to find the signal correspondence $\boldsymbol{C}$ between $\boldsymbol{G}$ and $\boldsymbol{P}$.

In contrast, *if the signal correspondence is known*, the relative sensor-orientation described by $\boldsymbol{R}$ can also be computed easily.

As such, this is a typical chicken-egg problem between finding signal correspondence and estimating relative sensor-orientation.

3. Orientation-Compensative Signal Matching Algorithm

3.1 Algorithm Overview

To solve the chicken-egg problem between relative
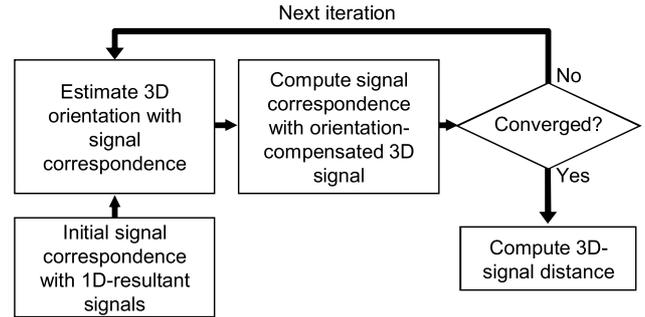

Fig. 2 Flowchart of the proposed orientation-compensative matching algorithm.

sensor-orientation and signal correspondence as stated in Sect. 2.2, we propose an iterative framework of signal correspondence based on cyclic dynamic programming and relative sensor-orientation estimation. The algorithm is started by initializing the signal correspondence (see Fig. 2).

From Sect. 2.2, we know that the sensor rotation changes the 3D signal $\boldsymbol{a}_i$, however, we observe that this rotation does not change the magnitude of the signal:

$$\|\boldsymbol{a}_i'\| = \sqrt{\boldsymbol{a}_i^T \boldsymbol{R}'^T \boldsymbol{R}' \boldsymbol{a}_i} = \sqrt{\boldsymbol{a}_i^T \boldsymbol{a}_i} = \|\boldsymbol{a}_i\| \quad \forall \boldsymbol{R}'. \tag{3}$$

Therefore, a sequence of magnitude $\{\|\boldsymbol{a}_i\|\}$ is a 1D resultant signal sequence that is invariant to initial sensor-orientation variation. Obviously, this can be used as the orientation-invariant feature for gait recognition [29], [35]. However, reducing the signal from 3D to 1D results in a significant loss of information.

For the 1D resultant signal sequences $\boldsymbol{G}_r = \{\|\boldsymbol{g}_i\|\}$ and $\boldsymbol{P}_r = \{\|\boldsymbol{p}_j\|\}$ of the original 3D gallery signal sequence $\boldsymbol{G}$ and probe signal sequence $\boldsymbol{P}$, respectively, the signal correspondence can be acquired by a cyclic dynamic programming without the sensor-orientation inconsistency problem. This prompts us to initialize the signal correspondence between $\boldsymbol{G}$ and $\boldsymbol{P}$, which is approximated by using $\boldsymbol{G}_r$ and $\boldsymbol{P}_r$.

We can use the same cyclic dynamic programming to register both the 3D orientation-compensated signals and the 1D resultant signals to compute the signal correspondence.

3.2 Signal Correspondence Acquisition by Cyclic Dynamic Programing

We consider the signal correspondence between a gallery signal sequence $\boldsymbol{G} = \{\boldsymbol{g}_i\}$ ($i = 0,\ldots,N_G-1$) and a probe signal sequence $\boldsymbol{P} = \{\boldsymbol{p}_j\}$ ($j = 0,\ldots,N_P-1$). In this subsection, the initial sensor-orientation inconsistency is not considered for these signal sequences or they are already orientation-compensated. The goal is to acquire a set of the signal correspondence pair $\boldsymbol{C} = \{\boldsymbol{c}_k\}$ ($k = 0,\ldots,N_K-1$) so as to match the gallery and probe signal sequences.

In our problem setting, the signal sequence length N_G of an individual gallery pattern is one gait period, while that of a probe pattern, N_P, is unconstrained. The signal correspondence $\boldsymbol{C}$ starts and ends by two pairs associated with the

initial and final samples, p_0 and p_{N_P-1}, of the probe signal sequence, respectively. Moreover, non-linear temporal distortion may contaminate the signal sequences. We therefore use a cyclic dynamic programming (CDP) which is modified from the standard DTW [36] using modular arithmetic to match these signals.

We first introduce an accumulated cost matrix $D_{N_G \times N_P} = \{D(i,j)\}$ $(i = 0,..,N_G - 1, j = 0,...,N_P - 1)$. Then, the dynamic programming is presented by four steps based on the accumulated cost matrix D: initialization, recursive update, termination, and backtracking to find the optimal path, which is used as signal correspondence C.

3.2.1 Initialization

The accumulated cost matrix is initialized:

$$D(i,0) = \|g_i - p_0\|, \quad \forall i = 0,..,N_G - 1. \tag{4}$$

3.2.2 Recursive Update

$$D(i,j) = \|g_i - p_j\| + \min_{(p,q)\in T} \{D((i-p) \bmod N_G, j-q)\}, \tag{5}$$

where mod N_G means residue by the gait period N_G and $T = \{(1,2),(1,1),(2,1)\}$, which means the double speed, same speed, and half speed transition steps for searching, respectively.

3.2.3 Termination

The end of the optimal path, minimizing the accumulated cost at the final sample p_{N_P-1} of the probe signal sequence, is found:

$$c_{N_K-1} = \left(\arg\min_{i=0}^{N_G-1} D(i, N_P - 1), N_P - 1\right). \tag{6}$$

3.2.4 Backtracking

The optimal path is recursively backtracked until j_k reaches the first sample of the probe signal sequence p_0:

$$(p^*, q^*) = \underset{(p,q)\in T}{\arg\min} D((i_{k+1} - p) \bmod N_G, j_{k+1} - q),$$
$$c_k = ((i_{k+1} - p^*) \bmod N_G, j_{k+1} - q^*). \tag{7}$$

In summary, given the gallery and probe signal sequences G and P, the *CDP* module returns the signal correspondence C as denoted by:

$$C = CDP(G, P). \tag{8}$$

To remove unnecessary computation and thus speed up a DTW, global constraint on the search space is widely used [36]. For a standard DTW, the initial and end points are known, the optimal path can be constrained by Sakoe-Chiba band [37] around the diagonal line of the accumulated matrix D. In our algorithm, the initial and end points

are not fixed, it is impossible to directly apply Sakoe-Chiba band. However, only after the initialization step, we know the initial optimal path C_0, and hence the Sakoe-Chiba band around C_0 is applied. The band size is 40% of the size of the matrix D, then we can save 60% of the computation cost.

3.3 Relative Sensor-Orientation Estimation

We first define a rotation matrix R as a function of a yaw-pitch-roll vector $r = [\alpha, \beta, \gamma]^T$, $R = R(r)$, where α, β, and γ mean *yaw*, *pitch*, and *roll* angles, respectively.

Given a signal correspondence C, we compute the yaw-pitch-roll vector r that minimizes the dissimilarity between the gallery signal sequence G and the orientation-compensated probe signal sequence $R(r) \odot P$ as:

$$r^* = \arg\min_r d(G, R(r) \odot P; C), \tag{9}$$

where $d(\cdot, \cdot; C)$ is a dissimilarity function based on normalized cross-correlation of two signal sequences given the signal correspondence C:

$$d(G, R(r) \odot P; C) = 1 - \frac{\sum_{(i,j)\in C} (g_i - \bar{g})^T R(r)(p_j - \bar{p})}{\sqrt{\sum_{(i,j)\in C} \|g_i - \bar{g}\|^2 \sum_{(i,j)\in C} \|p_j - \bar{p}\|^2}}, \tag{10}$$

and $\bar{g}$ and $\bar{p}$ are mean vectors of the gallery and probe signal samples associated with C, respectively. It should be noted that the standard deviation of a signal sequence is also invariant to initial sensor-orientation.

This problem is analogous to a simple rotation estimation from correspondence of 3D points in computer vision where each signal correspondence pair (g_i, p_j) is analogous to a correspondence pair of 3D points. One can find a large number of solutions for this problem such as those given in [38], [39]. In our experimens, we used the secant version of Levenberg-Marquardt least squares method implemented in [40].

3.4 Algorithm Summary and Example

Here, the orientation-compensative matching algorithm is summarized in pseudo code in **Algorithm** 1.

Algorithm 1 Gallery and Probe Signal Registration Algorithm

Input: The gallery and probe signal sequences G, P
Output: Rotation matrix R^* and signal correspondence C^*
  $C^0 = CDP(G_r, P_r)$ {Initialization step}
  $r^0 = \arg\min_r d(G, R(r) \odot P; C^0)$
  $k = 0$
  repeat
    $k = k + 1$
    $C^k = CDP(G, R(r^{k-1}) \odot P)$
    $r^k = \arg\min_r d(G, R(r) \odot P; C^k)$
  until C^k and r^k are converged
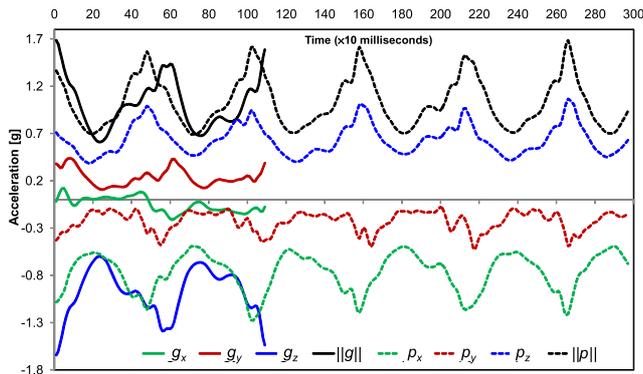 $R^* = R(r^k)$
  $C^* = C^k$

Fig. 3 Examples of the gallery sequence $\{(g_x, g_y, g_z)\}$ and probe sequence $\{(p_x, p_y, p_z)\}$. The gallery sequence contains 108 samples (1.08 second) of a single gait period, while the probe sequence contains 300 samples (3 second). $\{\|g\|\}$ and $\{\|p\|\}$ are their resultant signal sequences, respectively. Although the signal sequences are completely different due to the sensor-orientation inconsistency, their resultant signal sequences (depicted in black) are very similar.
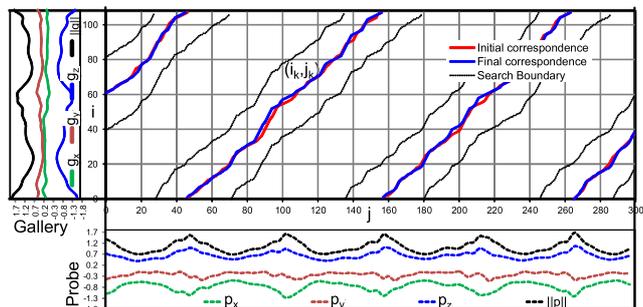

Fig. 4 The initial and final optimal paths computed by CDP are used as the signal correspondences between gallery and probe signals: C^0 and C^*. The boundary band for the search space is applied after C^0 has been estimated.

To find the initial correspondence $C^0 = CDP(G_r, P_r)$, CDP is executed only once for 1D orientation-invariant signals. However, to find the optimal correspondence C^*, several CDP procedures are performed to iteratively register the 3D signals.

To demonstrate the iterative matching procedure, we apply it to the 3D acceleration signal sequences and their resultant signal sequences, which are plotted in Fig. 3. The initial and final correspondences, C^0 and C^* computed by the dynamic programming are shown in Fig. 4. In the initialization step, the initial correspondence C^0 is computed, and the initial registration of 3D signal sequences shown in Fig. 5 (a). We can see that the signal sequences are completely different owing to the different sensor orientations, but the resultant signal sequences can be well-registered. In the final step, the correspondence C^* and orientation R^* are computed from the 3D signal sequences, and the signal registration is shown in Fig. 5 (b) after correcting the relative sensor rotation for the probe signal sequence using R^*. Now, we can see that both the 3D acceleration signal sequences and resultant signal sequences are well-registered. The dissimilarity between the signal sequences
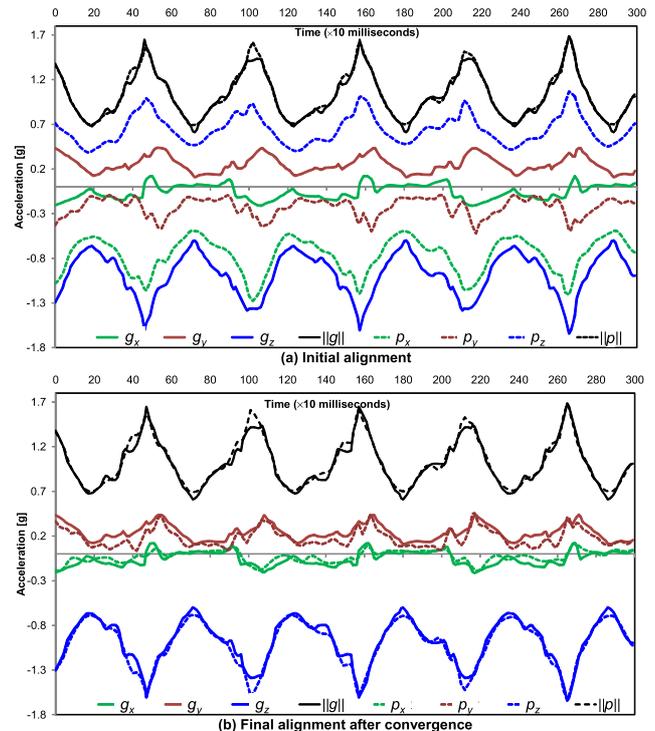

Fig. 5 Signal plot of the initial (a) and final (b) registration between the gallery and probe signals in Fig. 3. The alignments use C^0 and C^*, respectively. In (b), probe signal is rotated using estimated rotation matrix R^*, two signals are now well-registered and the dissimilarity (distance) between them can be now computed. In these figures, color denotes the individual dimension (x, y, z) or resultant signal (in black color), and line-style denotes the gallery (solid line) and probe (dashed line).

can be computed accurately. One should note that all the alignments in Fig. 5 are carried out along time axis j of the probe signal sequence.

4. Authentication

We use a simple authentication method to evaluate the orientation-compensative matching algorithm. A gallery $\mathbb{G}$ is defined as a collection of sample patterns for a subject taken under various conditions: $\mathbb{G} = \{G\}$. For any probe signal P, the distances between it and all the sample patterns in $\mathbb{G}$ are computed, and the minimum rule [41] is exploited to integrate results from multiple periods as:

$$Dist(\mathbb{G}, P) = \min_{G \in \mathbb{G}} d\left(G, R^* \odot P; C^*\right). \tag{11}$$

In fact, $d\left(G, R^* \odot P; C^*\right)$ is the dissimilarity function given by the rotation optimization function, Eq. (9).

5. Experiments

5.1 Setup

To capture 3D acceleration signals, our experimental system employed four accelerometers, including one of the latest sensors from MicroStrain Inc., the 3DM-GX3-25 [42]
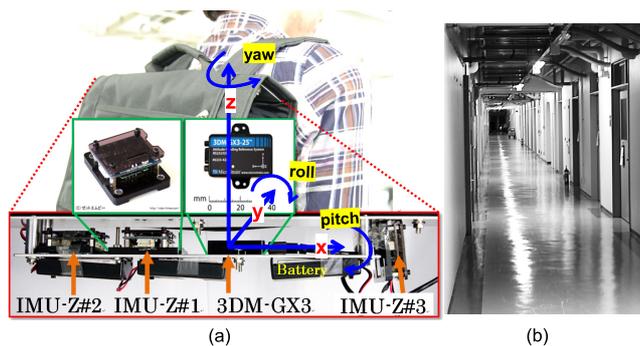
Fig. 6 The experimental setup includes (a) 4 sensors with different orientations and locations, and subject walks along an indoor corridor (b). Subject's body coordinate system is originated at the body center of mass, which consists of a vertical axis pointing upwards, lateral axis pointing from left to right, and longitudinal axis pointing from back to front. Body's *yaw*, *pitch*, and *roll* angles are rotation angles around the vertical, lateral, and longitudinal axes, respectively. The 3DM-GX3-25 is spatially about the center of sensor systems, its sensor coordinate system is set similar to the subject's body coordinate system.

and three IMU-Z sensors [43] from ZMP Inc. The sensors were fixed at different orientations and locations on the same plate placed under the handle and inside a backpack as shown in Fig. 6. The 3DM-GX3-25 was connected to a small computer, a Sony VAIO type P, through a USB connection, while the three IMU-Z sensors were connected through bluetooth connections. As the orientations and locations of the sensors differed, so too did the captured acceleration signals from these sensors. The orientations of IMUZ-1 and IMUZ-2 relative to the 3DM-GX3-25, expressed as (*yaw*, *pitch*, *roll*) angles, were fixed at (90, 180, 0) and (−180, 0, −180) deg, respectively. These angles were later used as ground-truth for evaluating the relative sensor rotation estimation. IMUZ-3 was fixed at an arbitrary orientation. The relative distances from IMUZ-1, IMUZ-2, and IMUZ-3 to the 3DM-GX3-25 were about 6, 11, and 12 cm, respectively. The sampling period for these sensors was 10 milliseconds.

5.2 Dataset

Since human gait varies as a result of many factors, the recognition performance also varies as pointed out in [35]. We therefore captured data under different conditions for evaluation. We captured a dataset using multiple sensors under different sensor-orientations, sensor-locations, days, and carrying weights in the backpack. The two total weights of the backpack were approximately 3 and 4 kg. 47 healthy subjects aged 21 to 50 years including 15 females and 32 males took part in the experiments and walked at their normal speed in a long straight corridor. We captured 16 sequences per subject (2 days × 2 carrying weights × 4 sensors) for 38 subjects and 8 sequences per subject (1 day × 2 carrying weights × 4 sensors) for the other 9 subjects. Each sequence was nearly 2 minutes long and contained about 64 gait periods (128 steps). The walking path was about 90 m

Table 1 Summary of benchmark methods.

Method denotation	Robustness to temporal distortion	Robustness to sensor orientation	Dimension of signal
PROPOSED	Excellent	Yes	3D
TRUNG2011 [21]	Excellent	No	3D
TRUNG2011_RLT	Excellent	Yes	1D
DERA2010 [26]	Good	No	3D
RONG2007 [24]	Good	No	3D
GAF2010HI [35]	Bad	Yes	1D
FELIX2012 [32]	Bad	No	3D

long and signals were not noise-filtered. For subjects who joined for different days, data was captured within a month and clothes and shoes might be different across the days.

In authentication experiments, galleries were captured only by the 3DM-GX3-25. The reason for this choice is that, in general motion of a rigid object, different points on the object have different acceleration signals, and the farther the distance between the points is, the larger the difference between the signals becomes. Moreover, a sophisticated experiment on the distance between sensors is out of scope of this paper. We therefore chose the 3DM-GX3-25, which was located at the position relatively close to the other three IMUZ sensors, to minimize such signal difference.

5.3 Benchmark Methods

We compared the proposed method, denoted as PROPOSED, with other six benchmark methods including five latest period detection-based methods (TRUNG2011, TRUNG2011_RLT, DERA2010, RONG2007, FELIX2012) and one frequency analysis-based method (GAF2010HI) as summarized in Table 1. Note that TRUNG2011_RLT is our modification of TRUNG2011, which uses 1D resultant signals instead of the original 3D signals for the invariance to the initial sensor-orientation.

We choose these benchmark methods by considering their performances mostly against two problems: the temporal distortion and sensor-orientation inconsistency.

Firstly, with regard to the temporal distortion, the period detection-based methods (TRUNG2011, TRUNG2011_RLT, DERA2010, and RONG2007) use DTW for this purpose. As far as we know, these are the best period detection methods to deal with the temporal distortion. In particular, TRUNG2011 and TRUNG2011_RLT employ Self DTW [44] to accurately detect a period without any heuristic information, that is the reason why TRUNG2011 and TRUNG2011_RLT have excellent properties for the robustness to the temporal distortion.

Secondly, with regard to the sensor-orientation inconsistency, TRUNG2011_RLT and GAF2010HI are invariant to sensor-orientation without using heuristic or prior knowledge. This is because TRUNG2011_RLT and GAF2010HI employ the orientation-invariant 1D resultant signals for matching.

However, besides TRUNG2011_RLT, there is no

existing method that is proposed to tackle both problems[†]. That is why TRUNG2011_RLT was considered, which was modified from one of the best existing period detection-based methods [34].

In addition, with regard to the robustness to signal noise, FELIX2012 is the latest period detection-based method that takes the advantage of a machine learning technique and thus is theoretically the most robust among these benchmark methods. While TRUNG2011_RLT and GAF2010HI use the 1D signal for the orientation-invariance, the other methods use 3D signals.

5.4 Evaluation Measure

The receiver operating characteristics (ROC) curve and equal error rate (EER) were computed for the performance evaluation of individual methods. The ROC curve shows the relationship between the false rejection rate (FRR), otherwise known as false non-match rate (FNMR), and false acceptance rate (FAR), otherwise known as false match rate (FMR), for the authentication scenarios [45], [46]. EER is an error at the tradeoff point where FRR (or FNMR) and FAR (or FMR) are equal on the ROC curve. To make a ROC curve for an authentication method, we compute a dissimilarity matrix for probe patterns versus gallery patterns for all the subjects. The lower the EER, the better the method performs.

We executed the authentication process for each individual gait pattern independently when computing the dissimilarity matrix.

5.5 Results

5.5.1 Examples of Period Detection

Examples of gait patterns constructed in the benchmark and proposed methods are shown in Fig. 7 for a signal sequene of a subject. Other examples of gait patterns are illustrated in Fig. 8 showing different conditions and sensors for the same subject as Fig. 7, which were constructed by [21] in the proposed method. Each graph shows the constructed patterns of the same condition (sequence), in which the mean and standard deviation of patterns are denoted as the bold and dashed lines, respectively. In Fig. 7, the standard deviation of constructed patterns shows the quality of period detection for all benchmark methods. In Fig. 8, the difference among the conditions and within the same condition can be seen by the mean and standard deviation, respectively.

5.5.2 Convergence of Proposed Method

In this experiment, we compared the proposed algorithm

[†]Concerning the period detection against sensor-orientation inconsistency, because we mainly focused on the signal matching part, period detection as a preprocessing was performed on the 1D resultant signal for DERA2010, RONG2007, and FELIX2012. This ensured that the period-detection performances of these methods were orientation-invariant.
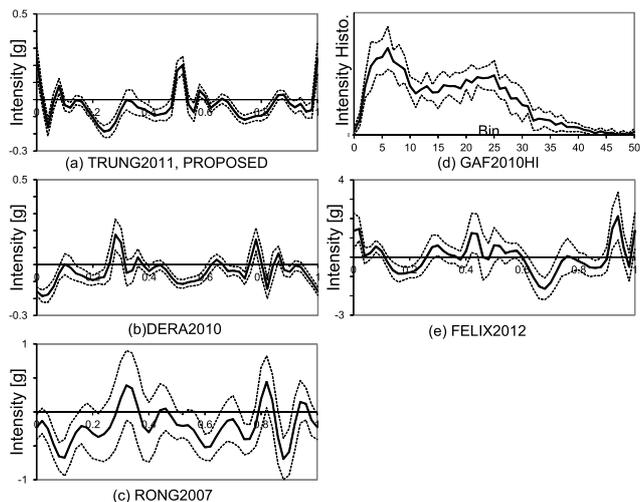
Fig. 7 Examples of constructed patterns only for acceleration on the y-axis captured by the 3DM-GX3-25: using PROPOSED or TRUNG2011 (a), using (b) DERA2010, (c) RONG2007, (e) the resultant intensity histogram of GAF2010HI, and (e) FELIX2012. For TRUNG2011_RLT, the period detection is the same as PROPOSED and TRUNG2011, a pattern is, however, constructed by computing the 1D resultant sigal. The distribution of patterns is represented by the mean (bold black line) and the standard deviation (dashed lines). Each gait pattern for the period detection-based methods was normalized to 50 samples per channel by re-sampling (PROPOSED, TRUNG2011, DERA2010, and FELIX2012) or by dynamically combining intensity-similar samples (RONG2007). In GAF2010HI, the number of histogram bins is limited by 50. For RONG2007, the signal intensity is normalized between [-1,1], and standard deviation of signal intensity for each channel is normalized to 1 in FELIX2012.
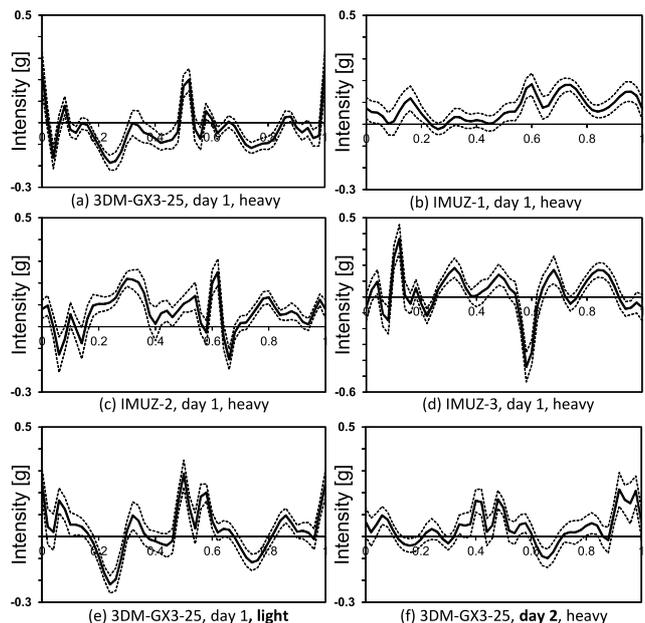
Fig. 8 Examples of acceleration gait patterns on the sensor's y-axis produced in the proposed method and captured under different conditions: different sensors ((a), (b), (c), and (d)) on the same day and with the same weight in the backpack; different weights in the backpack ((a) and (e)); and on different days ((a) and (f)). It should be noted that in (d) the signal intensity scale differs from that in the other graphs. The distribution of patterns is represented by the mean (bold black line) and the standard deviation (dashed lines).
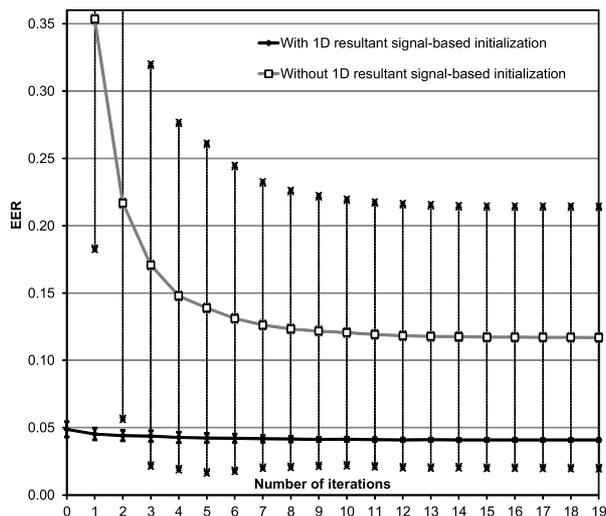
Fig. 9 Experiments with number of iteration for the proposed algorithm with and without 1D resultant signal-based initialization step. The standard deviation of EERs of the proposed algorithm with 1D resultant signal-based initialization was less than 0.0056.

Table 2 Computational cost for a matching pair.

Reference method	Computational cost [milliseconds]	Computational complexity versus pattern size (n)
PROPOSED with 10 iterations at most	12.4	$O(n^2)$
PROPOSED with 1 iteration at most	3.6	$O(n^2)$
DERA2010	1.3	$O(n^3)$
TRUNG2011, RONG2007, TRUNG2011_RLT	1.1	$O(n^2)$
GAF2010HI	0.0018	$O(n)$
FELIX2012	0.0176	$O(n)$

with and without 1D resultant signal-based initialization step. Without the 1D resultant signal-based initialization, the proposed algorithm has to carry out at least one iteration with the initial pitch-yaw-roll vector is set as $r^0 = (0, 0, 0)$ in the **Algorithm** 1. While with the 1D resultant signal-based initialization, the proposed algorithm can work without any iteration.

We used a subset of the dataset, a single sequence for each of the 47 subjects, captured on their first day by the 3DM-GX3-25. This data collection was divided equally into two sets to create the gallery and probe data, respectively. We computed EER for each number of iterations with and without 1D resultant signal-based initialization of signal correspondence. The average and standard deviation of EERs for proposed method are shown in Fig. 9 for 10 different random initial sensor orientations.

We can see that, without 1D resultant signal-based initialization, the algorithm was inaccurate and unstable because it was hardly able to reach the global minimum. However, with the 1D resultant signal-based initialization, the proposed algorithm was very robust against sensor-orientation variation, and the standard deviations of EER were less than 0.0056 for any number of iteration. Although the proposed algorithm can get a reasonable performance even just after the initialization, one or more iterations can give a more satisfactory accuracy.

In the remaining experiments, we set a convergence criterion on the difference of estimated rotation angles between two consecutive iterations (the matching process converged if the magnitude of the difference became less than 0.006 deg), and the number of iterations was limited by 10.

5.5.3   Computational Cost

The computational costs for all methods are shown in Ta-

ble 2 using the same dataset with Sect. 5.5.2. The table shows the average matching cost for a pair of gallery and probe patterns, which was computed on a pocket PC, Sony VAIO type P VGN-61S, with an Intel Atom Processor Z550, 2.0 GHz. GAF2010HI was the fastest method with linear computational complexity. FELIX2012 was the second fastest method also with linear computational complexity. Meanwhile, PROPOSED, TRUNG2011, RONG2007, TRUNG2011_RLT, and DERA2010 use DTW matching algorithm to improve the robustness to the temporal distortion, therefore they were slower than GAF2010HI and FELIX2012. Although using DTW matching, DERA2010 employs an additional procedure, the cyclic rotation metric (CRM) [26] to find the optimal shift between signals. Therefore, DERA2010 required longer processing time compared with TRUNG2011, TRUNG2011_RLT, and RONG2007. Among those methods, PROPOSED was the slowest since more processing time for solving the sensor-orientation inconsistency problem, although its computational complexity is the same as TRUNG2011, RONG2007, TRUNG2011_RLT.

Nevertheless, we can see that the computational cost for the proposed method is fast enough for a real-time application. In addition, we can speed up the proposed algorithm by setting a smaller number of iterations (e.g., speeded up from 12.4 ms at 10 iterations at most to 3.6 ms at 1 iteration at most in Fig. 9) with an insignificant performance drop. We also can improve the computational performance by applying the idea from FastDWT [47], which requires only linear time complexity in future.

5.5.4   Accuracy of Relative Sensor-Orientation Estimation

In this evaluation, we validate the relative sensor-orientation estimation in our algorithm. We compared the estimated sensor-orientation with the ground-truth orientation among the sensors. For each subject, gait patterns from IMUZ-1 and IMUZ-2 were compared with those from the 3DM-GX3-25 to estimate the relative sensor-rotation. For IMUZ-3, the experiment result was excluded since there was no ground-truth orientation. We used the same dataset with Sect. 5.5.2.

An orientation estimation error was computed when

Table 3   Relative sensor-orientation estimation results.

Comparison	Pitch error [deg]		Roll error [deg]		Yaw error [deg]	
	Mean	Std.dev	Mean	Std.dev	Mean	Std.dev
IMUZ-1 vs. 3DM-GX3	5.44	4.58	3.21	2.81	5.21	4.81
IMUZ-2 vs. 3DM-GX3	5.56	4.64	3.21	2.81	7.33	6.25

matching a gait pattern with its genuine gallery. The mean and standard deviation of the errors are shown in Table 3. From the table, we can see that the estimation error was approximately 7 deg at most for each axis. The accuracy is reasonable since our objective is to minimize the intensity difference between a pair of 3D signals. We also can see that the estimation error for *yaw* was more unstable than those for *pitch* and *roll*, and the estimation error for (3DM-GX3-25 vs. IMUZ-1) was smaller that that for (3DM-GX3-25 vs. IMUZ-2).
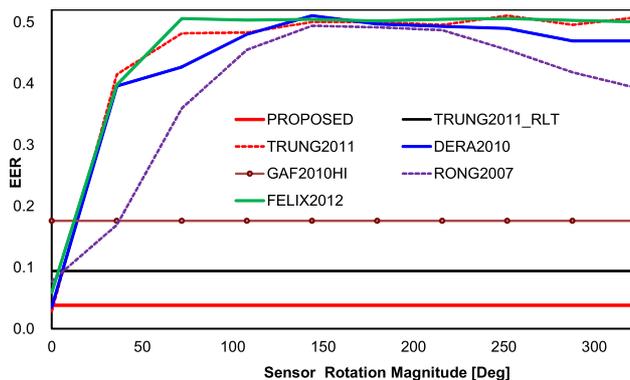
The reasons are explained as follows. Firstly, in the experimental setup, the coordinate system of the 3DM-GX3-25 almost coincided with the body coordinate system of a subject (see Fig. 6). For a normal gait motion, the vertical acceleration is dominated by the constant earth gravity, so that the vertical signal is much stronger and more stable than those of other two channels (Ox,Oy), as illustrated by the gallery signal captured by the 3DM-GX3-25 in Fig. 3. In addition, the vertical acceleration is relatively insensitive to the *yaw* angle, while it is very sensitive to *pitch* or *roll* angle. If we change a little *pitch* or *roll*, the vertical signal will be changed significantly. Therefore, the angle estimation by Eq. (9) tends to keep the dominant vertical acceleration signal of IMUZ sensor similar to that of the 3DM-GX3-25. As a result, this optimization keeps the *pitch* and *roll* errors quite smaller and sacrifices the *yaw* accuracy.

Secondly, although all the sensors were fixed in the same rigid board, the locations of the sensors differed. Therefore, the transformation between signals of different sensors for the same gait motion cannot be described by pure rotation; this is only true if the sensors are gyroscopes. Regardless of the sensor-orientation inconsistency, the farther the sensors are, the more different their signals become. That is why the orientation estimation errors for matching between the 3DM-GX3-25 and IMUZ-2 were greater than those for matching between the 3DM-GX3-25 and IMUZ-1. Another difficulty for the accuracy of orientation estimation is induced by difference of gait patterns themselves (e.g. different motions) of the same subject.

Despite of these difficulties, the accuracy for the relative sensor-orientation estimation is sufficient for our matching algorithm.

5.5.5   Simulated Sensor-Orientation Inconsistency

The experiment on simulated sensor-orientation inconsistency was carried out to focus on how the proposed and benchmark methods responded to the relative sensor rota-

Fig. 10   Performance of methods against varying simulated relative sensor-orientation.

tion. In this experiments, the dataset of the same 47 subjects as Sect. 5.5.2 was used.

The average results of EER of 10 random trials are shown in Fig. 10. From these results, we can see that TRUNG2011, FELIX2012, RONG2007, and DERA2010 worked well only without relative sensor rotation; as the relative orientation difference became larger, these methods failed, and hence they are unsuitable for real applications. Meanwhile, PROPOSED, TRUNG2011_RLT, and GAF2010HI were robust to sensor-orientation inconsistency, and PROPOSED achieving the best performance. Compared with PROPOSED, the results for TRUNG2011_RLT were inferior because the data dimension of the resultant signal was reduced from 3D to 1D. GAF2010HI uses a frequency analysis-based method, it requires a long stable signal sequence to compute a reliable histogram. Satisfying this requirement is in fact difficult, since human gait signals are unstable and are easily affected by many factors such as walking speed, mood, physical condition, and ground condition. Therefore, compared with TRUNG2011_RLT, GAF2010HI yielded worse results despite both methods using the resultant signal.

5.5.6   Real Sensor-Orientation Inconsistency

This experiment was carried out to validate the proposed method in real situations. We checked the authentication performance between the sensors with different orientations. All the data from the dataset were used in this experiment. Therefore, signals captured by the 3DM-GX3-25 were used to create the galleries and data from the other three sensors were used as the probes. This experiment demonstrated how effectively the proposed algorithm deals with the real sensor-orientation inconsistency. In this experiment, not only the effect of the sensor-orientation inconsistency between gallery and probe data, but also the relative sensor displacement were evaluated.

The experimental results, shown in Fig. 11 for ROC curves and Fig. 12 for EERs, are similar to those in Fig. 10 for large orientations. PROPOSED achieved the best EER and ROC curve, proving that it works well with variations in
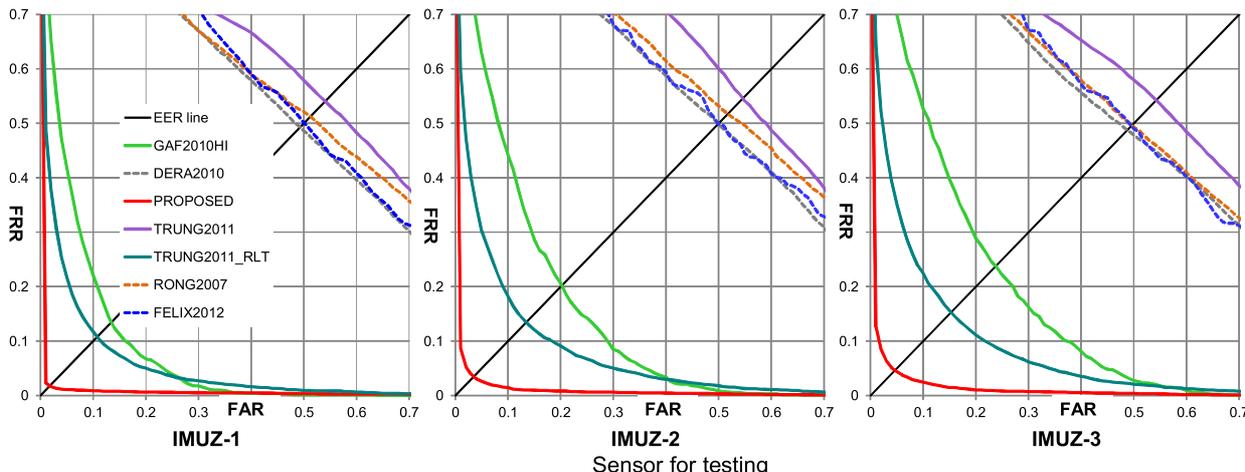
Fig. 11 ROC curves of the methods using different sensor data. Data from the 3DM-GX3-25 were used for making galleries, while those from the other sensors were used for testing. The same legends are used for all graphs.
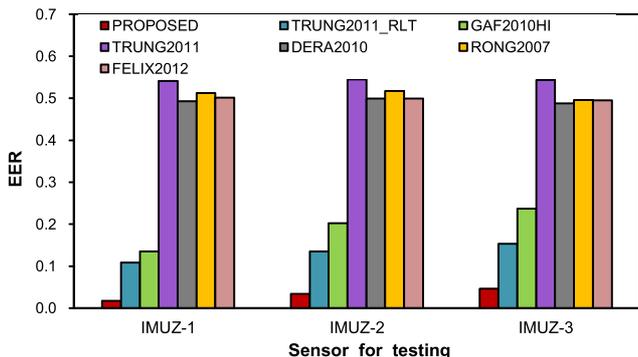

Fig. 12 EERs of the methods using different sensor data. Data from the 3DM-GX3-25 were used for making galleries, while those from the other sensors were used for testing.

the real sensor orientation. The EER values are 1.7, 3.4, and 4.6% for data from IMUZ-1, IMUZ-2, and IMUZ-3, respectively. Since the distance between IMUZ-1 and the 3DM-GX3-25 was small, the acceleration signals captured by two sensors were very close after orientation-compensation, resulting in a small EER for the test data from IMUZ-1. The differences in acceleration signals increased for more distant sensors, and hence the EERs for the test data from IMUZ-2 and IMUZ-3 were worse than that for IMUZ-1. This experiment also proved that the proposed method works well with a certain degree of sensor displacement, up to about 12 cm. As such, the proposed method could be a promising candidate for real application.

5.5.7 Overall Experiment

An experiment was carried out to evaluate the proposed method in a real application using the data captured on different days in the dataset. All the signals for the 38 subjects captured on their first day by the 3DM-GX3-25 were used as galleries, and all data captured by the 3DM-GX3-25,

IMUZ-1, IMUZ-2, and IMUZ-3 on their second day were used as probes.

The experimental results are shown in Fig. 13 for ROCs curves and Fig. 14 for EERs. The testing data captured by the 3DM-GX3-25 on the second day were the easiest to recognize for all the methods since no relative rotation and displacement occurred. The performance of RONG2007 is slightly better than that of TRUNG2011, and DERA2010. This is because RONG2007 applies an signal intensity normalization so that signal intensity fall within $[-1, 1]$, to overcome the problem of different intensity scales for gait signals for different walking speeds and physical conditions on different days. Meanwhile, FELIX2012 normalizes signal intensity so that standard deviation of signal intensity is 1 for each channel. The normalization in FELIX2012 is more robust than that in RONG2007. As a result, FELIX2012 gave a slightly better performance compared with that of RONG2007. Although using the same sensor and attachment configuration on the subjects for different days, signal intensity was varied not only by different clothes, shoes, mood or physical condition, but also by different subject's body tilt that caused the sensor-orientation inconsistency problem. Therefore, PROPOSED produced a better result compared with all other methods.

For testing data captured by all the IMUZ sensors, the results are similar to those in Figs. 11 and 12.

Overall, we can see that PROPOSED achieved the best results. We also can see that the recognition performance on different days is much worse than that in Sect. 5.5.6. This prompts us to ensure that gallery data are captured on different days and under varying conditions to cover as much variation as possible to improve the recognition performance in real applications.

6. Limitation and Discussion

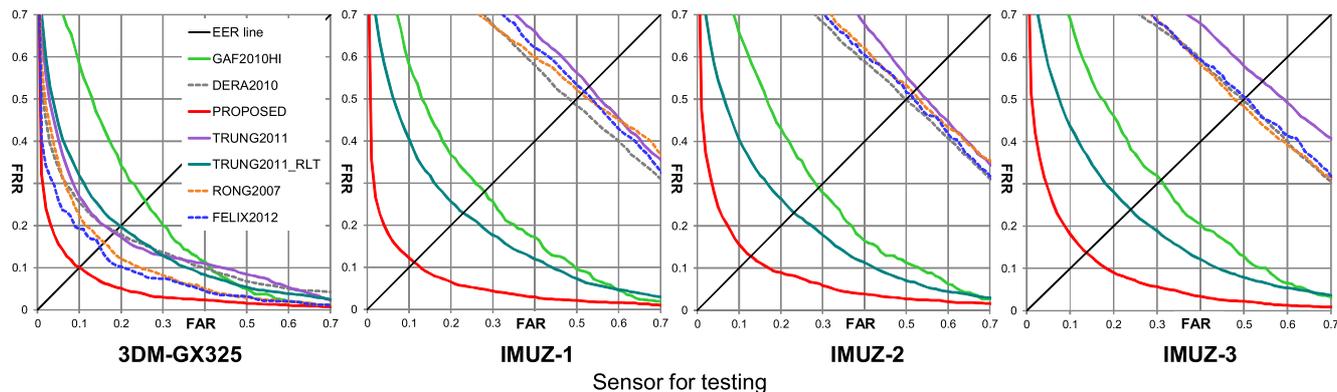Our system assumes that the sensor is fixed on the subject body during a short term (approximately 1 second) and com-

Fig. 13　ROC curves of the methods using different days. Data captured by the 3DM-GX3-25 on the first day were used to create the gallery, while data from all the sensors captured on the other day were used for testing. The same legends are used for all graphs.
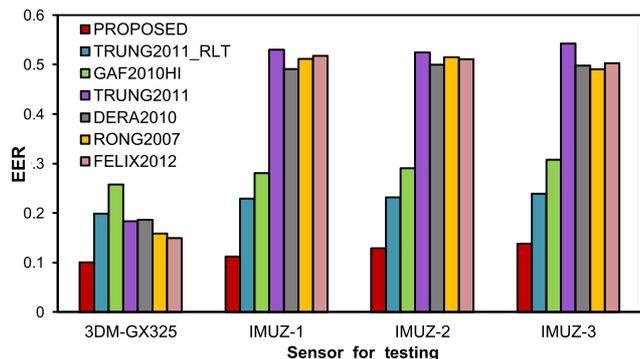

Fig. 14　EERs of the methods for different days. Data captured by the 3DM-GX3-25 on the first day were used to create the gallery, while data from all the sensors captured on the other day were used for testing.

pensates the sensor-orientation inconsistency for each short term independently. If the sensor moves (rotates and/or translates) freely and its motion within the short term is significantly large compared with the subject's motion (e.g., a mobile phone in a loose pocket or bag), proposed method does not work, as well as the existing methods.

However, the relative sensor rotation within a signal sequence can be effectively estimated by employing a gyroscope [48]. Recently, a gyroscope is often integrated together with an accelerometer in a smartphone. This solution is similar to a video stabilization technique in a commercial handycam integrated with a gyroscope. Employing a gyroscope is a simple and effective solution with low computational cost. However, this solution requires integration of angular velocities from the gyroscope. Hence, it would accumulate some amount of rotation error. Fortunately, the accumulation error within a short term is also negligible. In addition, the proposed method executes the orientation-compensation for every short subsequence of signal, thus it is not affected by the accumulation errors between different subsequences. As a result, the proposed method has a potential to cope with freely rotated signals in conjunction with the gyroscope in future.

How is about the idea of using a gyroscope instead

of using the proposed orientation-compensative matching algorithm to solve the orientation-inconsistency problem? The answer is negative. It is because gallery and probe signal sequences are basically independent in a recognition system and gyroscope can never correct initial orientation difference between two independently captured signal sequences.

Although we applied the proposed method only to verification scenarios (owner authentication, one-to-one matching), we can also apply it to identification scenarios (one-to-many matching, e.g., user identification for a shared device), which is also a future work.

7. Conclusions and Future Work

In this paper, we proposed a method for gait-based owner authentication using 3D signal registration. Iterative signal matching incorporating the phase-registration technique and the relative sensor-orientation estimation is employed to overcome the sensor-orientation inconsistency. The initialization of the iterative framework using the 1D resultant signal significantly reduces computational cost and ensures fast convergence of the iterative procedure.

Various experiments conducted on different days, under different sensors, and wearing weights in the backpack have proved that the proposed method improves signal matching and that the orientation-compensative signal matching method is effective.

In practical application in daily life, we need to prepare the gallery patterns for more condition variations such as health, ground, clothes, shoes, and mood variation. Although different conditions can influence the signal patterns, the physical body does not change and hence, the proposed algorithm is still able to work, as experienced from most biometric systems. If the test signal is captured under similar conditions to those of enrolled ones, it is possible to find a good match with high accuracy. Therefore, feasibility test in daily life considering such variations is one of important future work.

In case the initial sensor-orientation changes fre-

quently, we need to add a stabilization function to the proposed method in conjunction with a gyroscope. This is another future work to deploy a practical test system.

Acknowledgment

References

[1] N.T. Trung, Y. Makihara, H. Nagahara, Y. Mukaigawa, and Y. Yagi, "Inertial-sensor-based walking action recognition using robust step detection and inter-class relationships," 21st International Conference on Pattern Recognition, pp.3811–3814, 2012.

[2] Y. Xiao, D. Low, T. Bandara, P. Pathak, H.B. Lim, D. Goyal, J. Santos, C. Cottrill, F. Pereira, C. Zegras, and M. Ben-Akiva, "Transportation activity analysis using smartphones," Consumer Communications and Networking Conference (CCNC), 2012 IEEE, pp.60–61, Jan. 2012.

[3] Pebble Technology, "Pebble e-paper watch," 2013. [Online]. Available: http://getpebble.com/

[4] A. Avci, S. Bosch, M. Marin-Perianu, R. Marin-Perianu, and P.J.M. Havinga, "Activity recognition using inertial sensing for healthcare, wellbeing and sports applications: A survey," Intl. Conf. on Architecture of Computing Systems, Workshop Proc., pp.1–10, 2010.

[5] J.C. Augusto and C.D. Nugent, eds., Smart homes can be smarter, Springer-Verlag, Berlin, Heidelberg, 2006.

[6] S. Helal, S. Mitra, J.S. Wong, C.K. Chang, and M. Mokhtari, eds., Smart Homes and Health Telematics, 6th International Conference, ICOST 2008, Ames, IA, USA, June-July, 2008, Proceedings, ser. Lecture Notes in Computer Science, vol.5120, Springer, 2008.

[7] J.R. Kwapisz, G.M. Weiss, and S.A. Moore, "Cell phone-based biometric identification," Proc. of the IEEE 4th International Conference on Biometrics: Theory, Applications and Systems, pp.1–7, 2010.

[8] M.O. Derawi, C. Nickely, P. Bours, and C. Busch, "Unobtrusive user-authentication on mobile phones using biometric gait recognition," Proc. 6th International Conference on Intelligent Information Hiding and Multimedia Signal Processing, pp.306–311, 2010.

[9] M. Tanviruzzaman, S.I. Ahamed, C.S. Hasan, and C. O'brien, "ePet: When cellular phone learns to recognize its owner," Proc. 2nd ACM workshop on Assurable and usable security configuration, pp.13–18, 2009.

[10] E. Vildjiounaite, S.-M. Makela, M. Lindholm, R. Riihimaki, V. Kyllonen, J. Mantyjarvi, and H. Ailisto, "Unobtrusive multimodal biometrics for ensuring privacy and information security with personal devices," Proc. 4th International Conference Pervasive Computing, pp.187–201, 2006.

[11] D. Johnson and M. Trivedi, "Driving style recognition using a smartphone as a sensor platform," Intelligent Transportation Systems (ITSC), 2011 14th International IEEE Conference on, pp.1609–1615, Oct. 2011.

[12] J. Paefgen, F. Kehr, Y. Zhai, and F. Michahelles, "Driving behavior analysis with smartphones: Insights from a controlled field study," Proceedings of the 11th International Conference on Mobile and Ubiquitous Multimedia, ser. MUM '12, pp.36:1–36:8, ACM, New York, NY, USA, 2012. [Online]. Available: http://doi.acm.org/10.1145/2406367.2406412

[13] D. Gafurov, "A survey of biometric gait recognition: Approaches, security and challenges," Proc. Norsk informatikkonferanse, pp.1–12, 2007.

[14] N.F. Troje, "Decomposing biological motion: A framework for analysis and synthesis of human gait patterns," Journal of Vision, vol.2, pp.371–387, 2002.

[15] T.A. Wrena, G.E.G. III, S. Ounpuud, and C.A. Tucker, "Efficacy of clinical gait analysis: A systematic review," Gait & Posture, vol.34, no.2, pp.149–153, 2011.

[16] D. Sutherland, "The evolution of clinical gait analysis part III - Kinetics and energy assessment," Gait & Posture, vol.21, no.4, pp.447–461, 2005.

[17] J. Michalak, N. Troje, J. Fischer, P. Vollmar, T. Heidenreich, and D. Schulte, "The embodiment of sadness and depression gait patterns associated with dysphoric mood," Psychosomatic Medicine, vol.71, no.5, pp.580–587, 2009.

[18] H.J. Ailisto, M. Lindholm, J. Mantyjarvi, E. Vildjiounaite, and S.-M. Makela, "Identifying people from gait pattern with accelerometers," Proc. SPIE, vol.5779, pp.7–14, 2005.

[19] J. Mantyjarvi, M. Lindholm, E. Vildjiounaite, S.-M. Makela, and H. Ailisto, "Identifying users of portable devices from gait pattern with accelerometers," Proc. of the IEEE International Conference on Acoustics, Speech, and Signal Processing, vol.2, pp.973–976, 2005.

[20] A. Kale, N. Cuntoor, B. Yegnanarayana, A.N. Rajagopalan, and R. Chellappa, "Gait analysis for human identification," Audio– and Video–Based Biometric Person Authentication LNCS, pp.706–714, 2003.

[21] N.T. Trung, Y. Makihara, H. Nagahara, R. Sagawa, Y. Mukaigawa, and Y. Yagi, "Phase registration in a gallery improving gait authentication," Proc. IEEE/IAPR International Joint Conference on Biometrics, pp.1–7, 2011.

[22] D. Gafurov and E. Snekkenes, "Gait recognition using wearable motion recording sensors," EURASIP Journal on Advances in Signal Processing, pp.1–16, 2009.

[23] D. Gafurov, E. Snekkenes, and P. Bours, "Improved gait recognition performance using cycle matching," Proc. IEEE 24th International Conference on Advanced Information Networking and Applications Workshops, pp.836–841, 2010.

[24] L. Rong, Z. Jianzhong, L. Ming, and H. Xiangfeng, "A wearable acceleration sensor system for gait recognition," Proc. of the 2nd IEEE Conference on Industrial Electronics and Applications, pp.2654–2659, 2007.

[25] L. Rong, D. Zhiguo, Z. Jianzhong, and L. Ming, "Identification of individual walking patterns using gait acceleration," Proc. of the 1st International Conference on Bioinformatics and Biomedical Engineering, pp.543–546, 2007.

[26] M.O. Derawi, P. Bours, and K. Holien, "Improved cycle detection for accelerometer based gait authentication," Proc. 6th International Conference on Intelligent Information Hiding and Multimedia Signal Processing, pp.312–317, 2010.

[27] G. Trivino, A. Alvarez-Alvarez, and G. Bailador, "Application of the computational theory of perceptions to human gait pattern recognition," Pattern Recogn., vol.43, no.7, pp.2572–2581, 2010.

[28] A. Alvarez-Alvarez, G. Trivino, and O. Cordon, "Human gait modeling using a genetic fuzzy finite state machine," IEEE Trans. Fuzzy Syst., vol.20, no.2, pp.205–223, April 2012.

[29] D. Gafurov, K. Helkala, and T. Sondrol, "Biometric gait authentication using accelerometer sensor," J. Computers, pp.51–59, 2006.

[30] T. Kobayashi, K. Hasida, and N. Otsu, "Rotation invariant feature extraction from 3-D acceleration signals," Proc. of the International Conference on Acoustics, Speech, and Signal Processing, pp.3684–3687, 2011.

[31] S. Sprager and D. Zazula, "A cumulant-based method for gait identification using accelerometer data with principal component analysis and support vector machine," WSEAS Transactions on Signal Processing, vol.5, no.11, pp.369–378, 2009.

[32] F. Juefei-Xu, C. Bhagavatula, A. Jaech, U. Prasad, and M. Savvides, "Gait-id on the move: Pace independent human identification using cell phone accelerometer dynamics," IEEE 5th International Conference on Biometrics, pp.8–15, 2012.

[33] Y. Makihara, N.T. Trung, H. Nagahara, R. Sagawa, Y. Mukaigawa, and Y. Yagi, "Phase registration of a single quasiperiodic signal using self dynamic time warping," Proc. of the 10th Asian Conference

on Computer Vision, pp.667–678, 2010.

[34] N.T. Trung, Y. Makihara, H. Nagahara, Y. Mukaigawa, and Y. Yagi, "Performance evaluation of gait recognition using the largest inertial sensor-based gait database," Proc. 5th IAPR International Conference on Biometrics, pp.360–366, 2012.

[35] D. Gafurov, J. Hagen, and E. Snekkenes, "Temporal characteristics of gait biometrics," Proc. 2nd International Conference on Computer Engineering and Applications, pp.557–561, 2010.

[36] M. Muller, Information Retrieval for Music and Motion, ch. 4, Springer-Verlag, 2007.

[37] H. Sakoe and S. Chiba, "Dynamic programming algorithm optimization for spoken word recognition," in Readings in speech recognition, eds. A. Waibel and K.-F. Lee, pp.159–165, Morgan Kaufmann Publishers, San Francisco, CA, USA, 1990.

[38] N. Ohta and K. Kanatani, "Optimal estimation of three-dimensional rotation and reliability evaluation," Proc. 5th European Conference on Computer Vision, pp.175–187, 1998.

[39] B.K.P. Horn, H.M. Hilden, and S. Negahdaripour, "Closed-form solution of absolute orientation using orthonormal matrices," J. Optical Society of America A, vol.5, no.7, pp.1127–1135, 1998.

[40] M. Lourakis, "levmar: Levenberg-marquardt nonlinear least squares algorithms in C/C++." [Online]. Available: http://www.ics.forth.gr/%7Elourakis/levmar/

[41] J. Kittler, M. Hatef, R.P.W. Duin, and J. Matas, "On combining classifiers," IEEE Trans. Pattern Anal. Mach. Intell., vol.20, no.3, pp.226–239, 1998.

[42] MicroStrain Inc., "3DM-GX3®-25." [Online]. Available: http://www.microstrain.com/3dm-gx3-25.aspx

[43] ZMP Inc., "IMU-Z," in Japanese. [Online]. Available: http://www.zmp.co.jp/e-nuvo/jp/imu-z.html

[44] Y. Makihara, H. Mannami, and Y. Yagi, "Gait analysis of gender and age using a large-scale multi-view gait database," Proc. of the 10th Asian Conference on Computer Vision, pp.440–451, 2010.

[45] A. Jain, A. Ross, and S. Prabhakary, "An introduction to biometric recognition," IEEE Trans. Circuits Syst. Video Technol., vol.14, no.1, pp.4–20, Jan. 2004.

[46] A. Mansfield and J. Wayman, "Best practices in testing and reporting performance of biometric devices, version 2.01," National Physical Laboratory Report CMSC, vol.14, no.2, pp.1–36, Aug. 2002.

[47] S. Salvador and P. Chan, "Toward accurate dynamic time warping in linear time and space," Intell. Data Anal., vol.11, no.5, pp.561–580, Oct. 2007.

[48] R.E. Mayagoitia, A.V. Nene, and P.H. Veltink, "Accelerometer and rate gyroscope measurement of kinematics: an inexpensive alternative to optical motion analysis systems," Journal of Biomechanics, vol.35, no.4, pp.537–542, 2002.

Yasushi Makihara received the B.S., M.S., and Ph.D. degrees in engineering from Osaka University in 2001, 2002, and 2005, respectively. He is currently an Assistant Professor of the Institute of Scientific and Industrial Research, Osaka University. His research interests are gait recognition, morphing, and temporal super resolution.

Hajime Nagahara received the B.E. and M.E. degrees in electrical and electronic engineering from Yamaguchi University in 1996 and 1998, respectively, and the PhD degree in system engineering from Osaka University in 2001. He was a research associate of the Japan Society for the Promotion of Science (2001–2003). He was an assistant professor at the Graduate School of Engineering Science, Osaka University, Japan (2003–2010). He was a visiting associate professor at CREA University of Picardie Jules Verns, France, in 2005. He was a visiting researcher at Columbia University in 2007–2008. Since 2010, he has been an associate professor in faculty of information science and electrical engineering at Kyushu University. Computational photography, computer vision, and virtual reality are his research areas. He received an ACM VRST2003 Honorable Mention Award in 2003.

Yasuhiro Mukaigawa received his M.E. and Ph.D. degrees from University of Tsukuba in 1994 and 1997, respectively. He became a research associate at Okayama University in 1997, an assistant professor at University of Tsukuba in 2003, and an associate professor at Osaka University in 2004. He joined the MIT Media Lab as a visiting associate professor from 2009 to 2010. His current research interests include computer vision and computational photography.

Yasushi Yagi is the Director of the Institute of Scientific and Industrial Research, Osaka University, Ibaraki, Japan. He received his Ph.D. degrees from Osaka University in 1991. In 1985, he joined the Product Development Laboratory, Mitsubishi Electric Corporation, where he worked on robotics and inspections. He became a research associate in 1990, a lecturer in 1993, an associate professor in 1996, and a professor in 2003 at Osaka University. International conferences for which He has served as chair include: ROBIO2006 (PC), ACCV (2007PC,2009GC), PSVIT2009 (FC), ACPR (2011PC, 2013GC). He has also served as the Editor of IEEE ICRA Conference Editorial Board (2008–2011). He is the member of Editorial Board of International Journal of Computer Vision, the Editor-in-Chief of IPSJ Transactions on Computer Vision & Applications and the Financial Chair of Asian Federation of Computer Vision Societies. He was awarded ACM VRST2003 Honorable Mention Award, IEEE ROBIO2006 Finalist of T.J. Tan Best Paper in Robotics, IEEE ICRA2008 Finalist for Best Vision Paper, PSIVT2010 Best Paper Award, MIRU2008 Nagao Award and IPSJ Trans. on Computer Vision and Applications Outstanding Paper Award (2011). His research interests are computer vision, medical engineering and robotics. He is a fellow of IPSJ and a member of IEICE, RSJ, and IEEE.

Trung Thanh Ngo received his M.E and Ph.D. degrees from Osaka University in 2005 and 2010, respectively. He is currently working as a postdoctoral researcher in the Department of Intelligent Media, Institute of Scientific and Industrial Research, Osaka University. His research interests include pattern recognition, gait motion recognition, robot localization and 3D map building, omnidirectional vision, and statistical robust estimation methods.